Reaction channel contributions to the helion optical potential

Journal Item

Reaction channel contributions to the helion optical potential

R. S. Mackintosh*
School of Physical Sciences, The Open University, Milton Keynes, MK7 6AA, United Kingdom

N. Keeley†
National Centre for Nuclear Research, ul. Andrzeja Sołtana 7, PL-05-400 Otwock, Poland

(Received 6 November 2019; published 26 December 2019)

Background: The well-established coupled channel and coupled reaction channel processes contributing to direct reactions make particular contributions to elastic scattering that are absent from local density folding models. Very little has been established concerning the contribution of these processes to the optical model potentials (OMPs) for ^{3}He scattering. For studying such processes, spin-saturated closed shell nuclei such as ^{16}O and ^{40}Ca are particularly suitable target nuclei and the (^{3}He, ^{4}He) reaction is easily handled within conventional reaction theory because it avoids complications such as breakup.
Purpose: To establish and characterize the contribution to the ^{3}He-nucleus interaction generated by coupling to neutron pickup (outgoing ^{4}He) channels; also to study the contribution of collective states and identify effects of dynamical nonlocality from these couplings.
Methods: Coupled reaction channel (CRC) calculations, including coupling to collective states, will provide the elastic channel S-matrix S_{lj} resulting from the included processes. Inversion of S_{lj} will produce the local potential that yields, in a single channel calculation, the elastic scattering observables from the coupled channel calculation. Subtracting the bare potential from the CRC calculations yields a local and l-independent representation of the dynamical polarization potential (DPP). From the DPPs, because of a range of combinations of channel couplings, the influence of dynamically generated nonlocality can be identified.
Results: Coupling to ^{4}He channels systematically induces repulsion and absorption in the ^{3}He OMP and also a reduction in the rms radius of the real part. The repulsion and absorption is less for ^{208}Pb than for the lighter target nuclei although the qualitative effects, including the general undularity of the DPPs, are similar for all cases; therefore coupling to these channels cannot be represented by renormalizing folding model potentials. Evidence is presented for substantial dynamical nonlocality of the induced DPPs; for ^{40}Ca this modifies direct reaction angular distributions. The local equivalent DPPs for individual couplings cannot be added to give the overall DPP for the complete set of couplings. For the ^{208}Pb case, channel coupling *reduces* the reaction cross section although it increases it for ^{16}O, with ^{40}Ca an intermediate case.
Conclusions: The DPPs established here strongly challenge the notion that folding models, in particular local density models, provide a satisfactory description of elastic scattering of ^{3}He from nuclei. Coupling to neutron pickup channels induces dynamical nonlocality in the ^{3}He OMP with implications for direct reactions involving ^{3}He. Departures from a smooth radial form for the ^{3}He OMP should be apparent in good fits to suitable elastic scattering data.

DOI: 10.1103/PhysRevC.100.064613

I. INTRODUCTION

It has long been established that collective and reaction channel processes play an essential role in direct nuclear reactions [1]. These processes also make an important contribution to the simplest direct reaction: elastic scattering. This contribution is not represented in theories of the nuclear optical model based on local density models. The formal contribution of such processes to the nucleon optical model potential (OMP) is both nonlocal and l dependent [1–3]. The nonlocality referred to here is distinct from the nonlocality because of exchange processes and will be referred to as dynamical nonlocality in what follows. However, such processes can be represented as a local and l-independent contribution to the phenomenological OMP in a way briefly reviewed in Sec. II A.

In the present work we study the contribution to the ^{3}He OMP of coupling to transfer channels and collective excitations. The contribution of coupled reaction channels to the OMP was studied for protons (for recent contributions see [4–8]) and deuterons [9], but in both these cases many effects were omitted or treated incompletely. For example, in the case of the contribution of neutron pickup to proton scattering, the breakup of the deuteron was not taken into account in most cases. In this respect, the contribution of the coupling of ^{4}He channels to the ^{3}He OMP is favorable, and is studied in this

*raymond.mackintosh@open.ac.uk
†nicholas.keeley@ncbj.gov.pl

work, together with the contribution of collective excitation of the target nucleus. The contribution of neutron pickup coupling to the ^{3}He OMP was studied before [10], but that work was superseded by major improvements to coupled reaction channel (CRC) codes [11], with finite range coupling and nonorthogonality corrections now being included.

Elastic scattering OMPs for closed shell nuclei, that are fitted to data, often depart from global potentials. This was specifically established for ^{3}He projectiles by Pang *et al.* [12]. Moreover, elastic scattering angular distributions for closed shell target nuclei tend to have deeper minima, making them harder to fit with standard parametrized forms. These facts make scattering from such nuclei of particular interest in the quest to understand interactions between nuclei. Moreover ^{16}O and ^{40}Ca are both spin-saturated nuclei. The spin-orbit interaction for helion scattering is the subject of a theoretical and phenomenological review by Hanspal *et al.* [13]. These authors distinguish the contribution of the spin-saturated core and the contribution of the other target nucleons. This makes the interpretation of scattering from spin-saturated nuclei, such as ^{16}O and ^{40}Ca, more straightforward. The present study is largely based on these two target nuclei. Such $T = 0$ targets also facilitate the identification of consequences for isospin symmetry breaking, for example, by comparing ^{3}H and ^{3}He interactions. Certain surprising general features that emerged from the studies with ^{16}O and ^{40}Ca target nuclei might arguably be characteristic only for such light nuclei. This possibility led us to perform similar calculations involving the much heavier closed shell (but not $T = 0$) nucleus ^{208}Pb.

II. INELASTIC AND PICKUP CONTRIBUTIONS TO THE ^{3}He OMP

A. Determining coupling contributions to the OMP

The channel coupling contributions to the ^{3}He OMP are determined as follows: The elastic channel S-matrix S_{lj} from a coupled channel (CC) calculation (CC refers throughout to both collective and reaction channel couplings) is subject to $S_{lj} \rightarrow V(r) + \mathbf{l}\cdot\mathbf{s}V_{\rm SO}(r)$ inversion and the difference between the resulting potential and the "bare potential," the elastic channel potential of the CC calculation, is identified as a local representation of the dynamical polarization potential (DPP) because of the coupling; see Ref. [14] for more details.

In contrast to the local DPPs determined by inversion, the formal DPP is both l dependent and nonlocal; see Refs. [1–3,15]. This channel-coupling nonlocality is distinct from the nonlocality because of exchange [16], the consequences of which are commonly represented phenomenologically [17,18]. We refer to the nonlocality arising from channel coupling as *dynamical nonlocality*, and evidence for it will be presented in what follows, exploiting the nonadditivity of the local-equivalent DPPs as discussed in Refs. [14,15,19]. Some of the undulatory ("wavy") properties of the local and l-independent DPPs found by inversion can be attributed to the underlying l dependence of the formal DPP [1–3]. In what follows all CC calculations were performed with the code FRESCO [11].

The dynamical nonlocality generated by channel coupling has an important consequence: The local equivalent DPP because of the coupling to a number of states when included in a single CC calculation is not the sum of the local equivalent DPPs that would be found when each of the coupled states was included in a separate CC calculation; see Refs. [14,15] and also Ref. [19] for further discussion. The consequences of this motivate a number of the calculations described in this work. One immediate consequence is that the DPP because of a number of coupled states cannot be calculated as the sum of the DPPs because of each of the states coupled individually.

B. The coupling, inelastic, and (^{3}He, ^{4}He) transfer

1. *Scattering of 32 MeV ^{3}He from ^{16}O*

The contributions of coupling to the following states were studied.

(1) The $\frac{1}{2}^-$ ground state of ^{15}O; the Q value for pickup to this state is 4.9147 MeV.
(2) The $\frac{3}{2}^-$ state of ^{15}O at 6.176 MeV.
(3) The collective 3^- state of ^{16}O at 6.130 MeV.

The DPPs for coupling to the two pickup states were determined both for separate calculations and when included together in a single CC calculation. The collective coupling effect was also evaluated in a separate calculation and together with the pickup coupling. Of primary interest, of course, is the contribution to the DPP of all the couplings together. However, as well as the interest in the distinctive contributions of collective and transfer coupling, there is significance in the degree to which contributions to the DPP add (or, rather, do not add) together. As discussed in earlier works [14,15], the nonadditivity of such contributions to the local equivalent DPPs gives a measure of the dynamical nonlocality generated by the coupling.

It is possible to relate the effects on the spin-orbit DPP of coupling to specific spin states. A test case will be reported in which coupling to an artificial $\frac{1}{2}^-$ state with the same Q value and other characteristics as the $\frac{3}{2}^-$ state was included.

For the pickup calculations (frequently referred to as PU calculations) the $\langle ^4\mathrm{He} \mid ^3\mathrm{He} + n\rangle$ overlap, i.e., the $n + ^3$He binding potential and spectroscopic factor, were taken from Brida *et al.* [20]. For the targetlike overlaps, the $n + ^{15}$O binding potentials were taken from Flavigny *et al.* [21], the spectroscopic factors being adjusted to give the best description of the (^{3}He, ^{4}He) pickup data of Lui *et al.* [22], yielding values of $C^2S = 1.10$ and 2.07 for the transitions to the 0.0 MeV $1/2^-$ and 6.18 MeV $3/2^-$ states of ^{15}O, respectively. The exit channel ^{4}He + ^{15}O optical potentials were calculated using the global parameter set of Ref. [23]. For the inelastic excitations, the $B(E3; 0^+ \rightarrow 3^-)$ was taken from Ref. [24] and the corresponding nuclear deformation length δ_3 from Ref. [25]. The full complex remnant term and nonorthogonality correction were included in the PU calculations.

2. *Scattering of 33 MeV ^{3}He from ^{40}Ca*

We studied the contributions to elastic scattering of coupling to the following collective and pickup states.

Pickup coupling was included to all states of ^{39}Ca with spectroscopic factors greater than 0.1, as determined in the paper by Doll *et al.* [26], some 22 states in all. Data are available for (^{3}He, ^{4}He) pickup to the 0.0-MeV $3/2^+$, 2.47-MeV $1/2^+$, 5.13-MeV $5/2^+$, and 6.16-MeV $5/2^+$ levels of ^{39}Ca for an incident ^{3}He energy of 33 MeV [22]. The Q value for pickup to the ground state of ^{39}Ca is 4.9426 MeV.

Collective coupling was included to two states of ^{40}Ca: the 3^- state at 3.737 MeV and the 2^+ state at 3.9044 MeV.

Like the case of scattering from ^{16}O, the dynamical nonlocality generated by the coupling is probed by examining the additivity of various contributions, pickup and inelastic, to the local equivalent DPP.

The pickup calculations again used the $\langle ^4\text{He} \mid ^3\text{He} + n\rangle$ overlap of Brida *et al.* [20] while the $n + ^{40}$Ca binding potentials were taken from Doll *et al.* [26]. The corresponding spectroscopic factors were also taken from Doll *et al.* except for the transitions to the 5.13-MeV and 6.16-MeV $5/2^+$ levels of ^{39}Ca where the Doll *et al.* values had to be doubled to provide a good description of the data of Lui *et al.* [22] for (^{3}He, ^{4}He) pickup to these states. The exit channel $^4\text{He} + ^{39}$Ca optical potentials were calculated using the global parameter set of Ref. [23]. For the inelastic excitations, the $B(E3; 0^+ \rightarrow 3^-)$ and $B(E2; 0^+ \rightarrow 2^+)$ were taken from Refs. [24] and [27], respectively, and the corresponding nuclear deformation lengths, δ_3 and δ_2, were taken from Ref. [28].

3. Scattering of 33 MeV ^{3}He from ^{208}Pb

For this target we studied the contributions of coupling to the following states.

Pickup coupling to all six hole states of ^{207}Pb analyzed in the ^{208}Pb(p, d) work of Matoba *et al.* [29] was included, i.e., the 0.0-MeV $1/2^-$, the 0.570-MeV $5/2^-$, the 0.900-MeV $3/2^-$, the 1.633-MeV $13/2^+$, the 2.340-MeV $7/2^-$, and the 3.413-MeV $9/2^-$. The Q value for pickup to the ground state of ^{207}Pb is 13.2097 MeV. No data are available for ^{208}Pb(^{3}He, ^{4}He) pickup at the same energy as the elastic scattering data of Farooq *et al.* [30].

Collective coupling to the 2.615-MeV 3^- and 4.0854-MeV 2^+ states of ^{208}Pb was also included.

As for the previous two targets, the pickup calculations employed the $\langle ^4\text{He} \mid ^3\text{He} + n\rangle$ overlap of Brida *et al.* [20] while the $n + ^{207}$Pb binding potentials and spectroscopic factors were taken from Matoba *et al.* [29]. The exit channel $^4\text{He} + ^{207}$Pb optical potentials were calculated using the global parameter set of Ref. [23]. For the inelastic excitations, the $B(E3; 0^+ \rightarrow 3^-)$ and $B(E2; 0^+ \rightarrow 2^+)$ were taken from Refs. [24] and [27], respectively, and the corresponding nuclear deformation lengths, $\delta_3 = 0.59$ fm and $\delta_2 = 0.25$ fm, were obtained by adjusting to fit the ^{208}Pb(^{3}He, ^{3}He′) inelastic scattering data of Refs. [31] and [32] in separate CC calculations.

III. FITS TO ELASTIC SCATTERING DATA

In this study of the contributions of various combinations of collective and/or reaction channel couplings, the bare potentials for ^{3}He scattering from the ^{16}O, ^{40}Ca, and ^{208}Pb targets were determined by fitting the relevant elastic scattering differential cross sections and analyzing powers by searching on the potential parameters with all couplings included. These were couplings to all pickup states and all collective states of the ^{16}O, ^{40}Ca, and ^{208}Pb target nuclei, as listed in the previous section. For the ^{16}O case, the spin-orbit parameters were not searched on but fixed at the set D1 parameters of Lui *et al.* [33] because otherwise the fit to the differential cross section dominated the fit to the analyzing power, leading to pathological spin-orbit parameters. These bare potential parameters were then held fixed for all subsequent calculations.

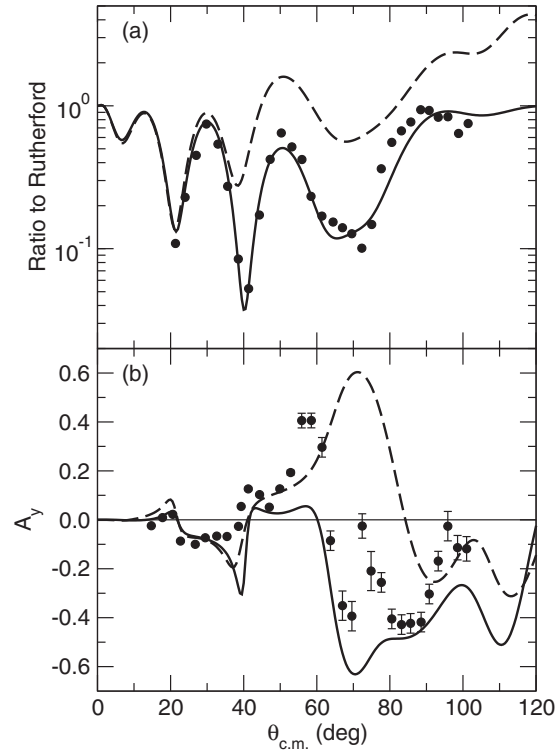

FIG. 1. For 32-MeV ^{3}He on ^{16}O, the solid lines are the differential cross section (above) and analyzing power angular distributions for the the full coupled channel calculation with fitted optical model parameters. The dashed lines are calculated with the same potential (the "bare potential") but with no coupling.

Figure 1 compares the fit to the elastic scattering of ^{3}He from ^{16}O with the couplings all switched on, solid lines, and with the bare potential (all couplings switched off), dashed lines. It will be seen that the fit to the analyzing power is imperfect, but these data have unusual features. In fact, as shown in Ref. [7], the actual DPPs are not very sensitive to the details of the bare potential so it is not critical to have perfect fits for determining the properties of the DPPs. Indeed, such fits involving many coupled reaction and inelastic channels have until recently been impractical and full searching on the many parameters of a model independent potential is not appropriate at present. The fit presented in Fig. 1 is better than the purely phenomenological OM fit of Lui *et al.* [33].

Figure 2 compares the fit to the elastic scattering of ^{3}He from ^{40}Ca with the couplings all switched on, solid lines, and with the bare potential (all couplings switched off), dashed

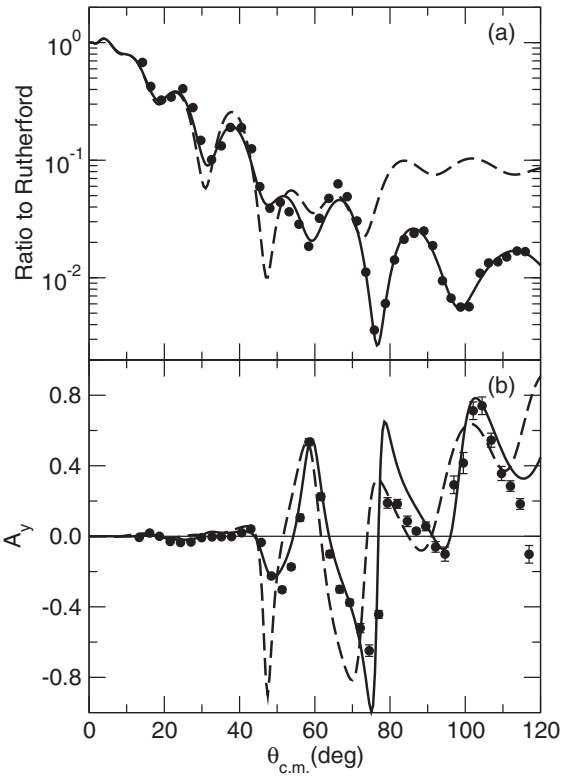

FIG. 2. For 33-MeV ^{3}He on ^{40}Ca, the solid lines are the differential cross section (above) and analyzing power angular distributions for the full coupled channel calculation with fitted optical model parameters. The dashed lines are calculated with the same potential (the "bare potential") but with no coupling.

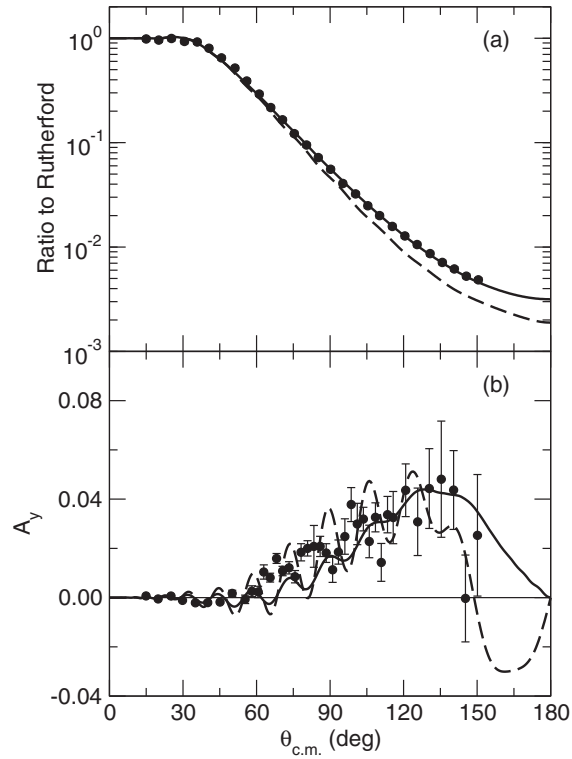

FIG. 3. For 33-MeV ^{3}He on ^{208}Pb, the solid lines are the differential cross section (above) and analyzing power angular distributions for the full coupled channel calculation with fitted optical model parameters. The dashed lines are calculated with the same potential (the "bare potential") but with no coupling.

lines. In this case the fits to both the angular distribution and the analyzing power are very good, apparently better than the single channel OM fits of Ref. [33], except for the analyzing power beyond 100°.

Figure 3 compares the fit to the elastic scattering of ^{3}He from ^{208}Pb with the couplings all switched on, solid lines, and with the bare potential (all couplings switched off), dashed lines. In this case the lack of structure reflects the absence of interference by a far side component. The shape of the small magnitude analyzing power is significantly modified by the coupling.

Finally, we present in Fig. 4 the potential obtained by inversion of the full CC calculation S matrix for the case of 33-MeV ^{3}He on ^{40}Ca. The dashed lines in this figure present the four components of the bare potential corresponding to the dashed lines in Fig. 2. The local potential that fitted the data, obtained by inversion and corresponding to the full set of channel couplings (pickup and inelastic), is given by the solid lines in Fig. 4. A full discussion of the channel couplings will be presented in what follows, but here we note three clear effects: (1) the real central potential was reduced overall, with an obvious reduction in its rms radius, (2) the wavy imaginary central potential has regions in the surface where it is emissive (without breaking the unitarity limit), and (3) a strong, complex spin-orbit interaction was generated. It looks nothing like the usual Thomas form of the standard phenomenology.

IV. EVALUATING THE DPPs

The local equivalent DPPs are determined by subtracting the components of the bare potentials from the corresponding components of the potential determined by inverting S_{lj} for the elastic channel of the particular CC case being studied. Characteristic properties of the DPPs for various combinations of the possible coupling are presented in Table I in terms of the differences between corresponding properties of the inverted and bare potentials. The radial forms for the DPPs for ^{3}He on ^{16}O are presented in Sec. IV A, for ^{3}He on ^{40}Ca in Sec. IV B and for ^{3}He on ^{208}Pb in Sec. IV C.

In Table I we employ the standard normalization of Ref. [1] for J_R and J_I, the volume integrals of the real and imaginary potentials. We also adhere to the standard sign convention, in which a positive sign represents attraction or absorption. Thus, a negative value for ΔJ_R represents a repulsive contribution from the particular coupling in question. To get a measure of the magnitude of coupling effects, note that for ^{3}He on ^{16}O the volume integrals of the real and imaginary terms of the bare (uncoupled) potentials were, respectively, $J_R = 421.46$ MeV fm^3 and $J_{IM} = 88.95$ MeV fm^3. The corresponding values for scattering from ^{40}Ca were $J_R = 398.47$ MeV fm^3 and $J_{IM} = 82.98$ MeV fm^3 and for scattering from ^{208}Pb were $J_R = 346.74$ MeV fm^3 and $J_{IM} = 66.18$ MeV fm^3.

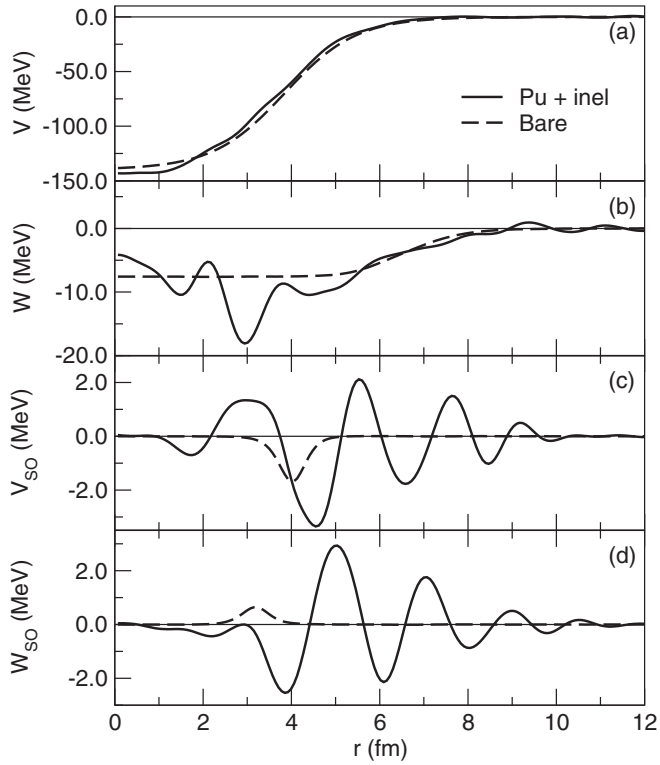

FIG. 4. For 33-MeV ^{3}He on ^{40}Ca, the bare potential (dashed lines) and the inverted potential including pickup and inelastic coupling contributions (solid lines). From the top downwards, the real central, imaginary central, real spin-orbit, and imaginary spin-orbit components.

For each case, Table I also presents Δ(Reac CS), the change in reaction cross section because of the coupling. The quantity R is the ratio of Δ(Reac CS) to $\Delta J_{\rm IM}$, the change, because of coupling, in the volume integral of the imaginary central potential:

$$R = \frac{\Delta(\text{ReacCS})}{\Delta J_{\rm IM}}. \quad (1)$$

R varies over a much smaller range than Δ(Reac CS) or $\Delta J_{\rm IM}$ separately.

Table I also presents the "State CS" which is the total (^{3}He, ^{4}He) and/or (^{3}He, ^{3}He′) cross section in mb to the pickup states and/or the collective states as specified in column 2. It gives a measure of the coupling and in some cases varies more than, and sometimes contrariwise to, the corresponding $\Delta J_{\rm IM}$.

Regarding the comparison of the DPPs for different couplings, it is important to note that all calculations for each target nucleus were carried out with a fixed bare potential, the potential that was determined by a search with all couplings included. The relative insensitivity of the DPP to the specific properties of the bare potential is presented in Ref. [7].

A. Radial forms of DPPs for ^{3}He on ^{16}O

Figure 5 presents the DPPs (i) for coupling to the pickup states (labeled "pu only"; dashed lines), (ii) for coupling to the collective states (labeled "inel only"; dotted lines), and (iii) for coupling to both the collective and transfer states, (labeled "pu + inel"; solid lines). There is no mutual coupling between the inelastic and pickup channels. The "pu" case exhibits a shallow attractive region near the origin, and repulsion between about 2 fm and 6 fm. The overall effect is a net repulsion, $\Delta J_{\rm R} = -24.58$ MeV fm^3 in line 5 of Table I, and a reduction in the rms radius of −0.041 fm. The dotted line shows that inelastic coupling alone gives a much stronger attractive region at the nuclear center but substantial repulsion around 5 fm, leading to overall repulsion and a corresponding decrease of the rms radius, −0.115 fm. When pickup and inelastic coupling are included together, the attraction at the nuclear center is less than for inelastic coupling alone, but the overall repulsion is increased as indicated by $\Delta J_{\rm R} = -55.58$ MeV fm^3 in line 7 of Table I, and, as in all cases reported in Table I, the rms radius decreases, in this case by 0.116 fm.

As might be expected the coupling increases the volume integral of the imaginary central potential, in this case (line 7) $\Delta J_{\rm IM}$ is just 16.03 MeV fm^3; this is conspicuously less than the sum, 40.18 MeV fm^3 of the increments $\Delta J_{\rm IM}$ because of pickup and inelastic coupling separately. This will be discussed in connection with Fig. 6 but we note here that both the inelastic and pickup coupling lead to somewhat undulatory (wavy) imaginary central components, the pickup DPP being less wavy than that because of inelastic coupling. This is a property that will also occur for the case of ^{40}Ca discussed below and to some degree for the case of ^{208}Pb.

We have seen that the volume integrals for the inelastic and pickup couplings do not add, and this applies point-by-point as shown in Fig. 6 which compares, for the four components, (i) the numerical sums of the local DPPs because of pickup and inelastic coupling, and, (ii) the local DPPs when both couplings are operative together. While the general shapes of the central terms are visually similar, the differences are sufficient to lead to the differences in the volume integrals in Table I, although the r^2 weighting in the volume integral makes visual judgment difficult.

The additivity of local DPPs was also studied for the pickup coupling to the $\frac{1}{2}^-$ and $\frac{3}{2}^-$ states of ^{15}O. The solid lines in Fig. 7 present the components of the local DPP for coupling when both states are included. The dashed lines present the local DPP for coupling to the $\frac{3}{2}^-$ state alone, and the dotted lines are for pickup to the $\frac{1}{2}^-$ state alone.

Figure 8 compares the components of the local DPP arising from coupling to both pickup states (solid lines) with the sum of the components of local DPPs for coupling to the $\frac{3}{2}^-$ and $\frac{1}{2}^-$ states independently (dashed lines). Again we find a significant difference which can be compared with the different values in lines 3 and 5 of Table I. In this case the general shapes of the "both" case components follow that for coupling to the $\frac{3}{2}^-$ state, which dominates, having much greater values of State CS and Δ(CS) than for the $\frac{1}{2}^-$ state, as given in Table I.

Part of the conspicuous difference between the $\frac{3}{2}^-$ and $\frac{1}{2}^-$ cases in Fig. 7 is because of the very different Q values and

TABLE I. For ^{3}He scattering from ^{16}O at 32 MeV, from ^{40}Ca at 33 MeV, and from ^{208}Pb at 33 MeV, volume integrals ΔJ (in MeV fm^3) of the four components of the DPP induced by (^{3}He, ^{4}He) pickup coupling ("PU") and/or coupling to inelastic states ("inel"). The coupled states for ^{16}O are specified in Sec. II B 1, those for ^{40}Ca in Sec. II B 2, and those for ^{208}Pb in Sec. II B 3; the excitation energies of the states, in MeV, are all specified. The $\Delta R_{\rm rms}$ column gives the change in rms radius of the real central component (in fm). The final three columns present, respectively, the change in the total reaction cross section induced by the coupling, the integrated cross section to the specific coupled reaction channels, and the ratio R defined in the text. Note that negative $\Delta J_{\rm R}$ corresponds to repulsion. The quantities Δ(CS) and State CS are given in mb.

Line	Label	Coupling	$\Delta J_{\rm R}$	$\Delta J_{\rm IM}$	$\Delta J_{\rm RSO}$	$\Delta J_{\rm IMSO}$	$\Delta R_{\rm rms}$	Δ(CS)	State CS	R
1	PU on ^{16}O	$\frac{1}{2}^-$	−6.02	3.607	−0.194	0.378	−0.033	18.6	11.27	5.16
2	PU on ^{16}O	$\frac{3}{2}^-$	−14.33	17.51	0.696	−0.509	−0.016	38.1	19.18	2.18
3	PU on ^{16}O summed	$\frac{1}{2}^-$, $\frac{3}{2}^-$	−20.35	21.12	0.501	−0.131	−0.048	56.7	30.45	2.69
4	PU on ^{16}O test	$\frac{1}{2}^-$ like $\frac{3}{2}^-$	−12.02	16.39	−0.639	1.790	−0.026	35.3	15.94	2.15
5	PU on ^{16}O	$\frac{1}{2}^-$ and $\frac{3}{2}^-$	−24.58	25.95	0.251	0.427	−0.041	48.4	25.64	1.87
6	Inel on ^{16}O	3^-	−46.86	14.22	0.188	0.461	−0.115	36.2	49.01	2.55
7	Inel and PU on ^{16}O	$\frac{1}{2}^-$ and $\frac{3}{2}^-$, 3^-	−55.58	16.03	0.907	0.385	−0.116	49.2	54.10	3.07
8	Inel and PU summed	$\frac{1}{2}^-$, $\frac{3}{2}^-$ and 3^-	−71.44	40.18	0.439	0.888	−0.156	84.6	74.65	2.11
9	PU on ^{40}Ca	See text	−15.81	33.47	1.022	0.837	−0.042	10.4	14.73	0.31
10	Inel on ^{40}Ca	See text	−24.74	34.31	0.104	−1.78	−0.117	−2.1	24.57	−0.25
11	Inel and PU on ^{40}Ca	See text	−36.62	16.95	1.755	−0.874	−0.157	1.9	36.06	0.011
12	Inel and PU summed		−40.55	67.79	0.918	−0.943	−0.159	8.3	39.30	0.122
13	PU on ^{208}Pb	See text	−2.33	6.286	0.520	−0.089	−0.603	−16.4	2.91	−2.6
14	Inel on ^{208}Pb	See text	−0.52	1.995	0.310	−1.088	−0.434	−1.4	4.90	−0.70
15	Inel and PU on ^{208}Pb	See text	−1.68	8.889	0.690	−0.869	−0.063	−18.0	7.88	−2.02
16	Inel and PU summed		−2.85	8.281	0.812	−1.177	−1.037	−17.8	7.81	−2.15

binding energies of the transferred neutron. It is of interest to relate the spin of the transferred neutron to the character of the contribution to the spin-orbit components of the DPP. To examine this, we compare in Fig. 9 three cases: (i) the DPP because of coupling to the $\frac{3}{2}^-$ state (dashed lines), (ii) the coupling to the $\frac{1}{2}^-$ state (dotted lines) and (iii) coupling to a test state (solid lines). The test state has spin $\frac{1}{2}^-$ but all other characteristics of the actual $\frac{3}{2}^-$ state. It will be seen that the character of the central components is generally similar to that for coupling to the actual $\frac{3}{2}^-$ state, so that these characteristics are dominated by the Q value, neutron form factor, etc. But this is not the case for the spin-orbit components, and indeed, the imaginary spin-orbit component is more like that for coupling to the $\frac{1}{2}^-$ state, so the effect on this component is dominated by the spin, as might have been expected.

B. Radial forms of DPPs for ^{3}He on ^{40}Ca

Figure 10 presents the DPPs for pickup to the states specified in Sec. II B 2. The dashed lines present the DPPs because of coupling to the pickup states; the dotted lines are for inelastic coupling to the vibrational states and the solid lines represent the components of the DPP when both inelastic and pickup couplings are included, with no mutual couplings between the collective and transfer channels. Certain general properties found in the ^{16}O case recur: Concerning the real central term, both couplings generate attraction at the nuclear center but, as seen in Table I, the overall effect is repulsive. As for ^{16}O the attraction near $r = 0$ is greater for the inelastic coupling than for the pickup coupling, but the total effect in that region is less when both couplings are effective.

The inelastic coupling actually generates a DPP that is emissive from the center to 3 fm but, as can be seen from Table I, the effect on the volume integral is as strongly absorptive as the pickup term.

It is clear that the pickup and inelastic DPPs are of different character, and a full representation of the coupling effect requires the inclusion of both kinds of coupling. However, inelastic and transfer DPPs cannot be calculated separately and then added. This can be seen in Fig. 11 which compares the sum of the pickup and inelastic DPPs with the DPP when both couplings are included together. This is very significant because this nonadditivity is a direct consequence of the dynamical nonlocality of the underlying DPPs, of which the DPPs presented here are the local equivalents.

While the inversion process yields DPPs with significant magnitudes at radii down to $r = 0$ it is legitimate to pose the question: Does the potential near the nuclear center matter for ^{3}He on ^{40}Ca at 33 MeV? It is reasonable to ask whether features in the region of $r = 0$ of the potential in Fig. 4 (see also Fig. 10, solid line) could have a significant effect on scattering. To answer this, we present Fig. 12 which compares the angular distribution for the full potential of Figs. 4 and 10 with the angular distributions when the same potential has deep notches in the real part at 0.48 and 0.98 fm. The notches

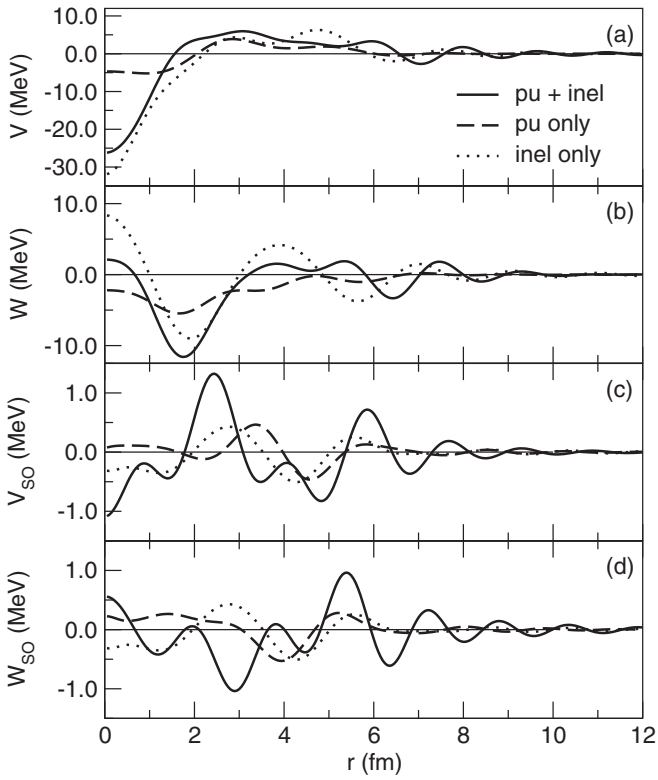

FIG. 5. For 32 MeV ^{3}He on ^{16}O, the DPPs for coupling to the 3^{-} collective state "inel" (dotted lines); to the 2 pickup states "pu" (dashed lines); and both couplings (solid lines). Components from top down: real central, imaginary central, real spin orbit, and imaginary spin orbit.

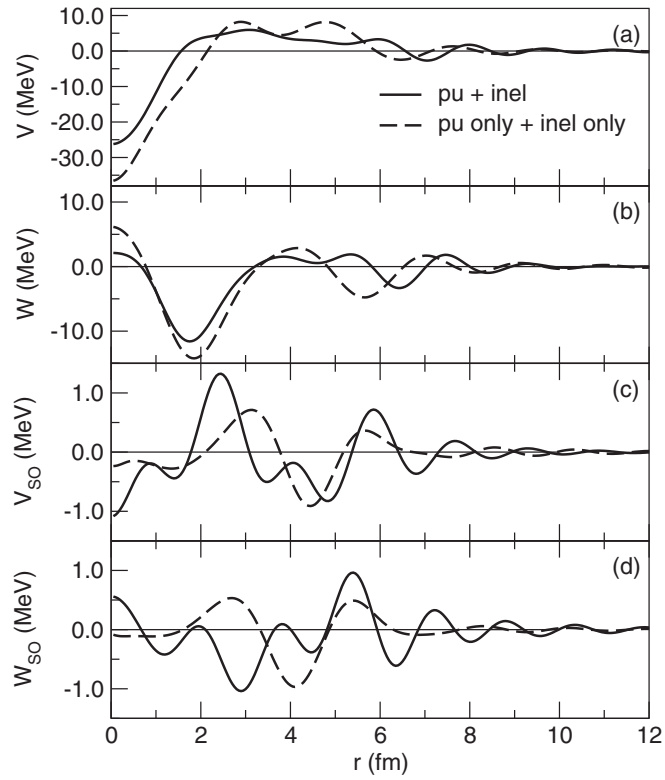

FIG. 6. For 32 MeV ^{3}He on ^{16}O, the solid lines present the DPP for coupling to both the pickup and collective states. The dashed lines present the numerical sums of the DPPs generated by each (collective or pickup) coupling separately. Components from top down: real central, imaginary central, real spin orbit, and imaginary spin orbit.

were of Gaussian form with width 0.025 fm and depth equal to the full potential at the central point of the notch. Because the full potential was tabulated in steps of 0.07 fm this amounted to almost V-shaped notches.

From Fig. 12 we see that for ^{40}Ca there is substantial sensitivity around 1 fm and appreciable sensitivity even at 0.5 fm. This suggests that the radial shape of the DPP presented in Fig. 10 is a realistic representation of the effect of channel coupling almost to the nuclear center.

C. Radial forms of DPPs for ^{3}He on ^{208}Pb

Figure 13 presents the DPPs for pickup to the states specified in Sec. II B 3. The dashed lines present the DPPs because of coupling to the pickup states, the dotted lines are for inelastic coupling to the vibrational states, and the solid lines represent the components of the DPP when both inelastic and pickup couplings are included, with no mutual couplings between the collective and transfer channels. The strong undulations in the real and imaginary central terms between 5 and 7 fm have the appearance of some kind of interference between the pickup and inelastic contributions. A notch test reveals sensitivity in the real part down to about 1 fm with some sensitivity out to 14 fm. There is substantial sensitivity in the imaginary potential only beyond 8 fm, but there is substantial sensitivity between 8 and 14 fm. This may be linked to the fact that the notch strength is related to the potential, and this is of surface character for the imaginary central term.

The extent to which the pickup and inelastic contributions add is shown in Fig. 14. Comparing with Fig. 11 it can be seen that the contributions add for the ^{208}Pb target somewhat better than was the case for the ^{40}Ca target. The relationship between the the contributions to the central potential has many similarities to the relationship for the corresponding quantities with the ^{40}Ca target.

D. General properties of the DPPs.

As will be seen in Figs. 5–11 and 13–14, all components of the DPPs have some degree of undularity, with some local regions where the imaginary terms become emissive. This does not lead to any breaking of the unitarity limit.

Here we note systematic properties revealed in Table I and Figs. 5–11 and 13–14.

(1) In broad terms, both coupling to inelastic channels and to pickup channels induces repulsion (negative ΔJ_{R}) and absorption (positive ΔJ_{IM}). However, the r dependence of the contributions because of inelastic and pickup coupling are systematically different, and both are very far from representing a uniform renormalization of the bare potential.

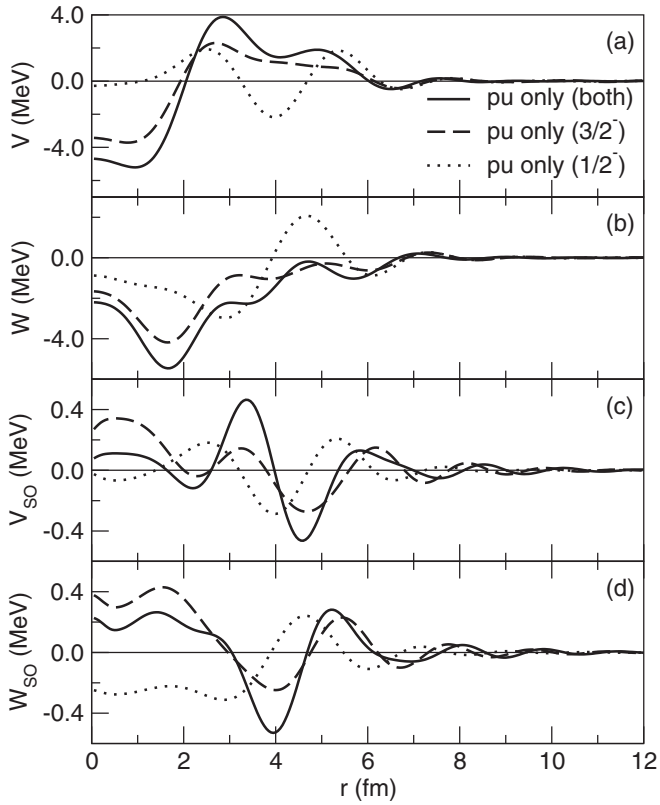

FIG. 7. For 32 MeV ^{3}He on ^{16}O, the solid lines present the DPP for coupling to both the $\frac{1}{2}^-$ and $\frac{3}{2}^-$ states of ^{15}O. The dashed lines present the DPPs generated by coupling to the $\frac{3}{2}^-$ state and the dotted lines represent coupling to the $\frac{1}{2}^-$ state of ^{15}O. Components from top down: real central, imaginary central, real spin orbit, and imaginary spin orbit.

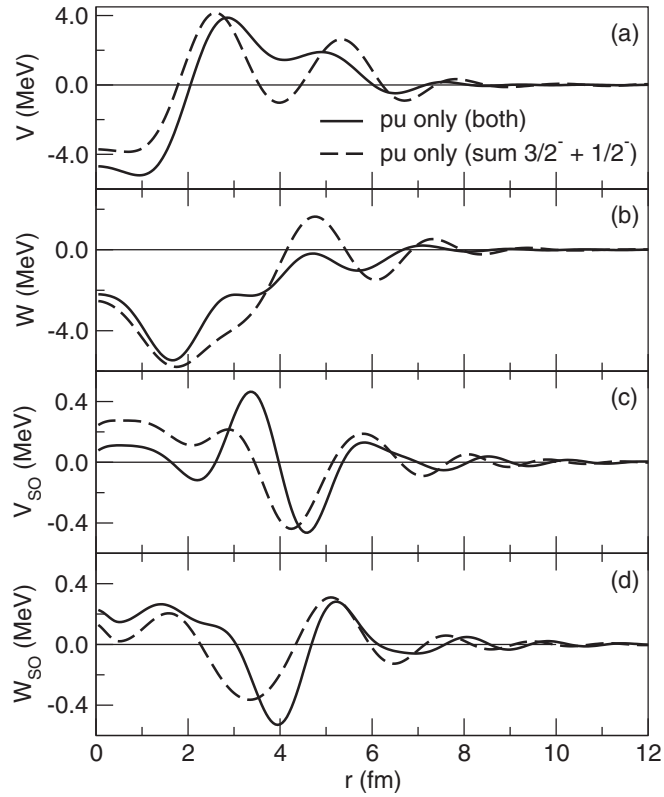

FIG. 8. For 32 MeV ^{3}He on ^{16}O, the solid lines present the DPP for coupling to both the $\frac{1}{2}^-$ and $\frac{3}{2}^-$ states of ^{15}O. The dashed lines present the numerical sum of the DPP generated by coupling to the $\frac{3}{2}^-$ state and the DPP generated by coupling to the $\frac{1}{2}^-$ state of ^{15}O. Components from top down: real central, imaginary central, real spin orbit, and imaginary spin orbit.

(2) In all cases the coupling (inelastic, pickup, or both together) causes a reduction in the rms radius of the real central term, i.e., $\Delta R_{\rm rms} < 0$. This is actually the opposite to the very systematic behavior found for protons on ^{40}Ca. This is relevant to the extraction of nuclear sizes using nuclear scattering.

(3) Comparing the effects for pickup from ^{16}O, the changes in both $\Delta J_{\rm RSO}$ and $\Delta J_{\rm IMSO}$ are opposite in sign for coupling to the $\frac{1}{2}^-$ and $\frac{3}{2}^-$; the strengths are in line with the multiplicity (larger for $\frac{3}{2}^-$) although the difference in the Q values also has an effect.

(4) Line 4 of Table I reports the test case in which the coupling is to a $\frac{1}{2}^-$ state having the binding energy and Q value of the $\frac{3}{2}^-$ state. The values of $\Delta J_{\rm R}$, $\Delta J_{\rm IM}$, Δ(CS), and R are close to the values for coupling to the $\frac{3}{2}^-$ state, while $\Delta J_{\rm RSO}$ and $\Delta J_{\rm IMSO}$ have the same signs as for coupling to the $\frac{1}{2}^-$ state, but much larger magnitudes.

(5) For ^{16}O and ^{40}Ca, the value of Δ(CS) when two channels or sets of channels are coupled simultaneously (but without mutual coupling) is less than the sum of the Δ(CS) values when the channels are coupled in separate calculations. This is true in the three cases in Table I: Compare lines 3 and 5, lines 7 and 8, and lines 11 and 12 of the table.

(6) In contrast to the last item the Δ(CS) values add quite closely for the ^{208}Pb target nucleus. For this case, however, the coupling *reduces* the total cross section, Δ(CS) being negative in lines 13–16.

(7) The same is true for the magnitudes of the volume integrals in the case where inelastic and PU coupling are combined (lines 7 and 8 and also lines 11 and 12) but not where PU channels are combined (lines 3 and 5).

(8) The small magnitude of $\Delta J_{\rm IM}$ in lines 7 and 11 is remarkable. In other cases, adding coupled states has generally increased the magnitude of $\Delta J_{\rm IM}$, but that is not the case leading to line 11. In this respect the ^{16}O and ^{40}Ca cases are very similar. The effect is very different for ^{208}Pb where the couplings acting together result in a slightly greater $\Delta J_{\rm IM}$.

(9) The contributions of inelastic and pickup coupling for ^{16}O are qualitatively very different. While in both cases the effect is repulsion (real term) and absorption (imaginary term) the magnitude of $\Delta J_{\rm R}$ for inelastic coupling is much larger than for $\Delta J_{\rm IM}$ whereas for pickup coupling the magnitudes are about the same,

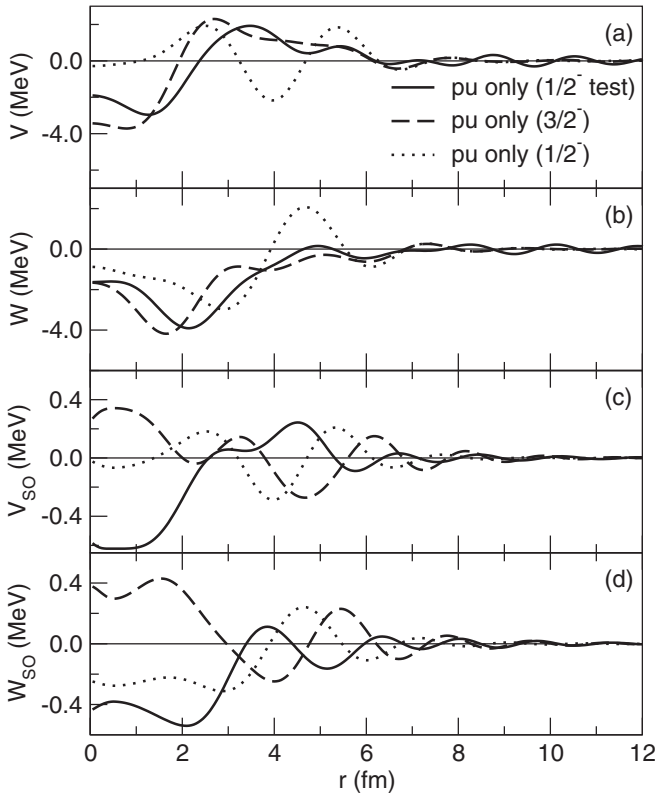

FIG. 9. For 32 MeV ^{3}He on ^{16}O, the dashed lines present the DPP for coupling to the $\frac{3}{2}^-$ state of ^{15}O and the dotted lines present the DPP for coupling to the $\frac{1}{2}^-$ state of ^{15}O. The solid lines present the DPPs for the test case in which the coupling was to a $\frac{1}{2}^-$ state with the Q value and other properties of the $\frac{3}{2}^-$ state. Components from top down: real central, imaginary central, real spin orbit, and imaginary spin orbit.

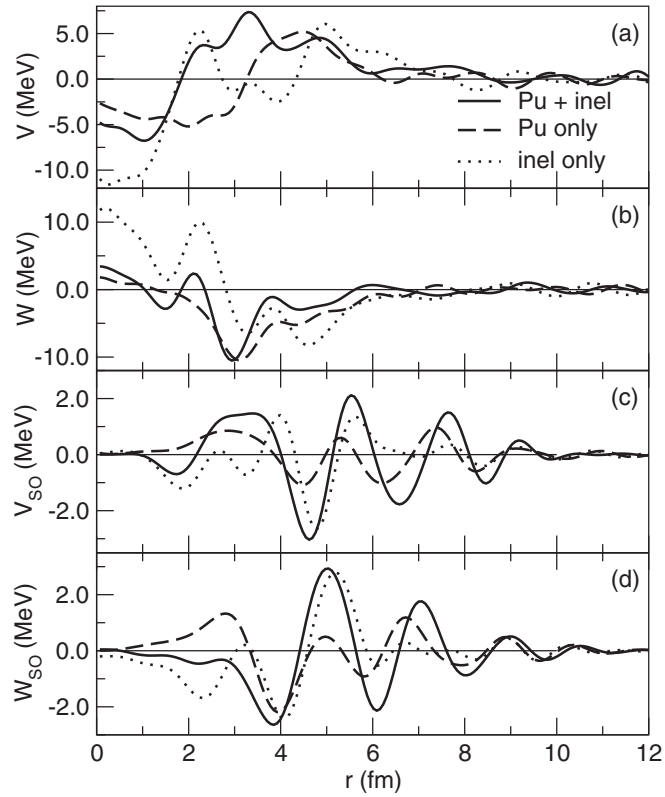

FIG. 10. For 33 MeV ^{3}He on ^{40}Ca, the DPPs for coupling to the collective states (see text) "inel" (dotted lines); to the pickup states "pu" (dashed lines); and both couplings (solid lines). Components from top down: real central, imaginary central, real spin orbit, and imaginary spin orbit.

with a particularly large repulsive effect on the real part.

(10) Quite unexpected in the ^{16}O case is the fact that the contribution to the imaginary DPP of pickup coupling and inelastic coupling acting together is considerably less than the pickup coupling alone. This is reflected in the fact that the value of Δ(CS) is hardly greater than for pickup coupling alone (49.2 mb, c.f. 48.4 mb).

(11) A similar effect, even more extreme, applies in the ^{40}Ca case: Again we find repulsion and absorption (in terms of volume integrals) but in this case the magnitude of $\Delta J_{\rm IM}$ when both inelastic and pickup coupling are included is considerably less (a factor of 4) than the sum of the separate inelastic and pickup contributions.

(12) The "together" values of State CS are systematically less than the "summed" values. Excitations of multiple channels evidently mutually suppress. This is particularly marked for the ^{16}O target. Is this a known effect?

The first point, together with the general undularity of the DPPs, exposes what is lost by fitting folding model potentials to elastic scattering data by uniform renormalization.

E. J dependence of the DPP for ^{16}O

For the ^{16}O case we have presented the effects of pickup to $\frac{1}{2}^-$ and $\frac{3}{2}^-$ states separately and together. Because the values of the change in the volume integral of the real spin-orbit term $\Delta J_{\rm RSO}$ are not of obvious significance, we calculate the ratio $\Delta J_{\rm RSO}/J_{\rm RSO}$ which is -0.065 for pickup to the $\frac{1}{2}^-$, 0.236 for pickup to the $\frac{3}{2}^-$, 0.085 for pickup to the $\frac{1}{2}^-$ and $\frac{3}{2}^-$, 0.063 for inelastic coupling, and 0.307 for full inelastic plus pickup coupling (ratios based on $J_{\rm RSO} = 2.951$ MeV fm^3 for the bare potential). In this light, most of the individual contributions are not large, with the $\frac{1}{2}^-$ and $\frac{3}{2}^-$ contributions tending to cancel (as might be expected) with the $\frac{3}{2}^-$ contribution (from 4 target nucleons) dominating. The final result that the complete contribution is about 30% shows that the contributions are not straightforwardly additive because of the general nonadditivity of nonlocal potentials.

V. THE DYNAMICAL NONLOCALITY OF THE DPPs

In this work we have stressed the fact that the DPP generated by coupling is nonlocal, and that the DPPs that we have

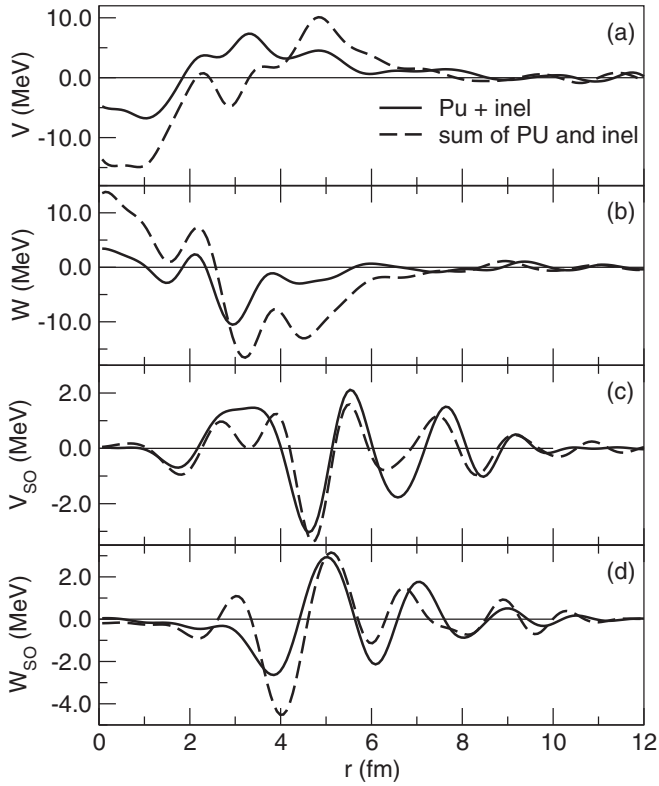

FIG. 11. For 33 MeV ^{3}He on ^{40}Ca, the solid lines present the DPP for coupling to both the pickup and collective states. The dashed lines present the numerical sum of the DPPs generated by each (collective or pickup) coupling separately. Components from top down: real central, imaginary central, real spin orbit, and imaginary spin orbit.

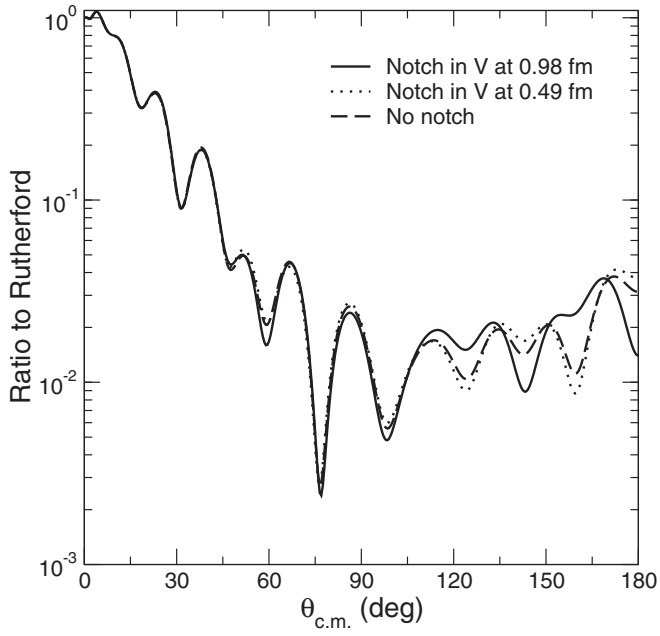

FIG. 12. For 33 MeV ^{3}He on ^{40}Ca, the angular distribution with the full potential without notch (dashed line), the angular distribution for the same potential but with a notch at 0.49 fm (dotted line), and with a notch at 0.98 fm (solid line).

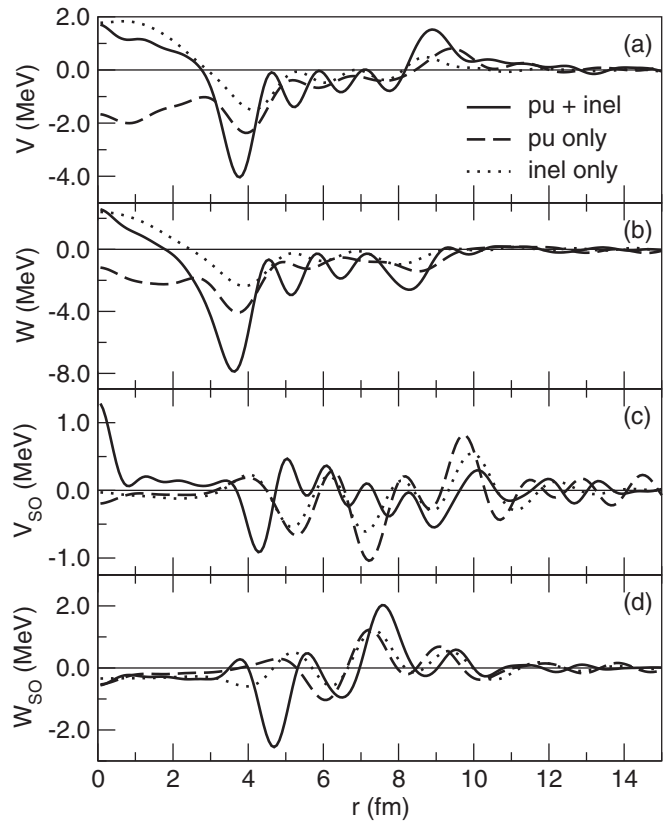

FIG. 13. For 33 MeV ^{3}He on ^{208}Pb, the DPPs for coupling to the collective states (see text) "inel" (dotted lines); to the pickup states "pu" (dashed lines); and both couplings (solid lines). Components from top down: real central, imaginary central, real spin orbit, and imaginary spin orbit.

presented are their local equivalents and thus correspond to the contribution of the particular couplings to the local OMP. Local OMPs are the product of most local density model folding calculations, and these generally lead to somewhat smooth radial forms. The phenomenological representations of such an OMP are, of course, a key ingredient in DWBA analyses of transfer reactions. There is now considerable literature on the effects of exchange-generated nonlocality in direct reactions, but the dynamically generated nonlocality is quite distinct from nonlocality induced by exchange. In spite of its obvious significance for direct reactions, dynamical nonlocality has been little studied; for exceptions (see Refs. [14,15]); for further discussion, particularly of the nonadditivity property see Ref. [19] where the additivity of the formal nonlocal DPPs is demonstrated.

In the present work, the consequences of dynamical nonlocality have already been seen in the nonadditivity of local DPPs. However, a comparison of (^{3}He, ^{4}He) DWBA stripping calculations in which the ^{3}He propagates alternatively in a dynamically nonlocal potential or in the local equivalent potential provides a direct indication of the effects of dynamical nonlocality otherwise evidenced only by the nonadditivity of the local DPPs. This comparison sends a message about the importance of dynamical nonlocality in the analysis of direct reactions.

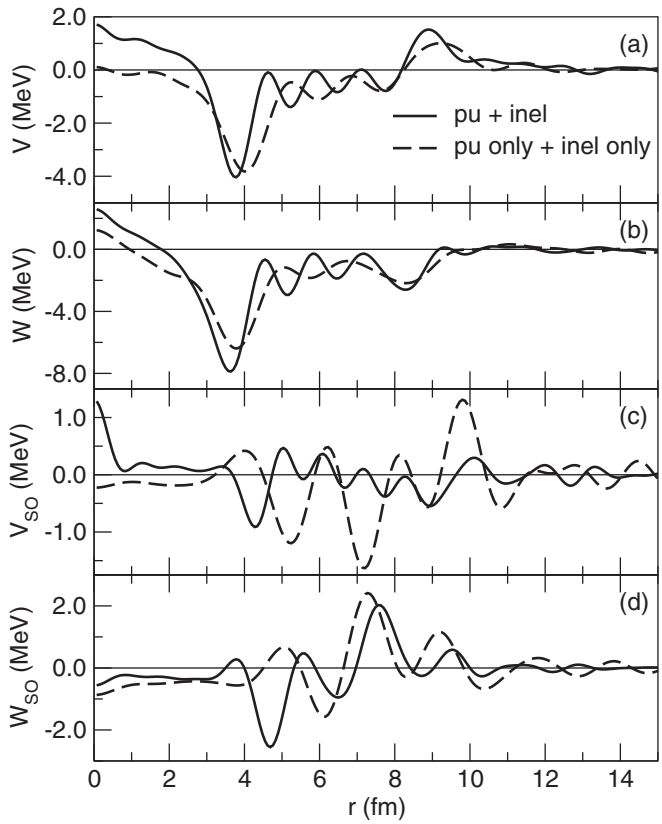

FIG. 14. For 33 MeV ^{3}He on ^{208}Pb, the solid lines present the DPP for coupling to both the pickup and collective states. The dashed lines present the numerical sum of the DPPs generated by each (collective or pickup) coupling separately. Components from top down: real central, imaginary central, real spin orbit, and imaginary spin orbit.

A difficulty in making a comparison would, in general, be the need to calculate the ^{3}He wave function in the presence of a nonlocal potential, and this would appear to involve solving an integro-differential equation, perhaps iteratively. This difficulty can be obviated by exploiting the fact that the wave function generated by the nonlocal DPP is, in fact, present in the CC calculations that generate the coupling. This can be exploited in the FRESCO [11] code by adding one-way pickup coupling between the ^{3}He wave function, effectively subject to a dynamically nonlocal potential, and a ^{4}He wave function in the exit partition.

This works out as follows in the example we present here. We consider a DWBA (^{3}He, ^{4}He) calculation on ^{40}Ca in which the ^{3}He wave function is calculated in two alternative ways: (i) in a coupled channel calculation in which the elastic channel is coupled to the 2^+ and 3^- states of ^{40}Ca as in the calculations reported above, and (ii) as propagating in the local potential that includes the local equivalent to the implicit DPP because of the same coupling. We have done this for two states of ^{39}Ca: (1) the $\frac{3}{2}^+$ ground state (Q value $+4.9426$ MeV) and (2) the $\frac{5}{2}^+$ state at 8.19 MeV (Q value -3.2474 MeV). Thus in this case the dynamical nonlocality is that from the coupling of the two collective states only and not from PU processes. Note that the ^{3}He elastic scattering observables are identical for both calculations.

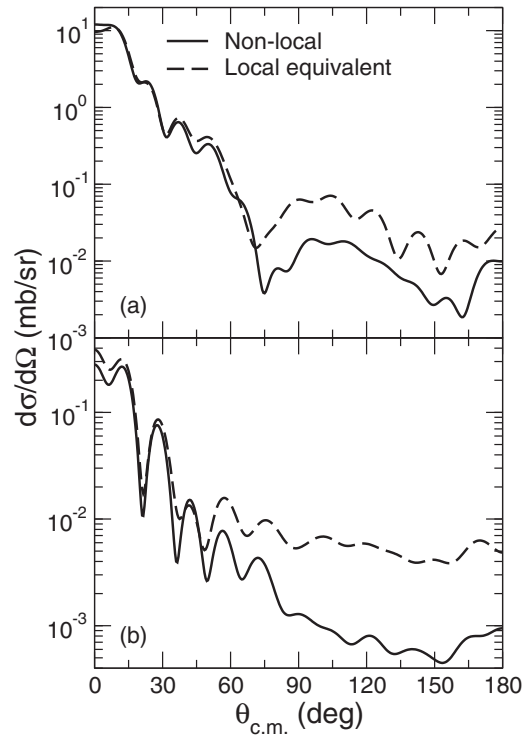

FIG. 15. For 33 MeV ^{3}He on ^{40}Ca, comparing DWBA calculations of (^{3}He, ^{4}He) stripping in which (i) the ^{3}He propagates in a dynamically nonlocal potential (solid lines) and (ii) the ^{3}He propagates in the local equivalent (dashed lines). The upper panel is for neutron pickup leading to the $\frac{3}{2}^+$ ground state of ^{39}Ca and the lower panel is for pickup to the $\frac{5}{2}^+$ state of ^{39}Ca.

Results of this comparison are presented in Fig. 15. The upper panel presents the angular distributions for pickup leading to the $\frac{3}{2}^+$ ground state and the lower panel presents the comparison for pickup leading to the $\frac{5}{2}^+$ state at 8.19 MeV. In each case, the solid line corresponds to the helion propagating in a dynamically generated nonlocal potential and the dashed line is for ^{3}He propagation in the local equivalent potential. In the case of the ground state, the substantial difference in angular distribution starts at about 30°. In the case of the $\frac{5}{2}^+$ excited state, the difference occurs at all angles and at the pickup peak around 9° the solid line (nonlocal) is depressed by about 20%. If one demands a fit at all angles for assurance that the transfer calculation delivers accurate spectroscopic information, then even for the ground-state case, the difference is significant. However, for the excited state case, where the deeper regions of the wave function are being probed, the result is plainly significant for the extraction of spectroscopic factors.

This case simultaneously demonstrates the reality of dynamically generated nonlocality and provides evidence of its significance in the analysis of direct reactions.

VI. OMITTED PROCESSES

The contribution of (^{3}He, ^{4}He) coupling is relatively straightforward to evaluate because the effects of ^{4}He

breakup, or other processes affecting the outgoing channel, are not expected to be great. That is not true of stripping channels. For example, for a ^{40}Ca target, an outgoing deuteron will couple to breakup channels and various other channels. A further complication is that much of the stripping strength in this case must go to unbound states. These are at present not straightforward to include in CRC calculations. Preliminary calculations for the ^{40}Ca target suggest that coupling to just the single bound state of ^{41}Sc makes a significant contribution to the ^{3}He OMP. That and further couplings must await a separate study.

VII. SUMMARY AND CONCLUSIONS

In this work, we have applied well-established coupled reaction channel methodology together with inverse scattering techniques to determine the contribution of channel coupling to the ^{3}He OMP for ^{16}O, ^{40}Ca, and ^{208}Pb. The particular channel couplings studied were pickup, i.e., (^{3}He, ^{4}He), and coupling to strongly excited inelastic channels. In the most general terms, we have shown that the ^{3}He optical model potential has significant contributions that are not part of any standard folding model based on a local density approximation. This constitutes a strong challenge to the notion that folding models, in particular local density models, provide a satisfactory description of elastic scattering of ^{3}He from nuclei.

Although the contributions to the OMP arising from channel coupling are l dependent and also dynamically nonlocal, we have presented here the l-independent and local equivalents. It is these that are relevant to comparisons with phenomenology, folding models, etc. Their characteristics, such as volume integrals and rms radii are presented in Table I. In fact, the couplings systematically decrease the rms radius of the real central potential and might thus modify the estimation of nuclear size from nuclear scattering. The dynamical nonlocality is significant for direct reaction spectroscopy; the effects, while being relatively calculable for ^{3}He scattering (Sec. V), suggest general properties relevant to all nuclear reactions. Unlike the nonlocality that arises from exchange processes, there are no known simple corrections for dynamical nonlocality. One consequence of the dynamical nonlocality is that the local equivalent DPPs for particular couplings cannot be added to give the total effect when such couplings operate together (without mutual coupling). This may be related to other apparently anomalous results that have arisen, such as the fact that the changes in reaction cross sections also do not add when independent couplings are switched on [refer to Δ(CS) in Table I].

Another effect, probably related, is the fact that cross sections for particular reaction channels depend on what other *not mutually coupled* channels are included in the calculation ("State CS" column of Table I); thus particular inelastic cross sections are sensitive to the presence of other reactions, even when there is no coupling between the respective channels. Although the change in the imaginary volume integral when couplings are switched on indicates that channel coupling generates an overall absorptive component in the OMP, the absorption is far from radially uniform, often leading to radial regions where the absorption is decreased, sometimes to the extent that the resulting imaginary potential may have emissive regions, though never leading to a breaking of the unitarity limit.

The nature of the DPPs presented here implies that folding models should be tested by model independent additive terms fitted to precise and wide angular range data, and not by applying a uniform renormalization [34].

When Satchler wrote his masterly review [1], direct reaction physics was already a mature subject, but 36 years later there remain surprises and many questions to be answered.

[1] G. R. Satchler, *Direct Nuclear Reactions* (Clarendon Press, Oxford, 1983).
[2] H. Feshbach, Ann. Phys. **5**, 357 (1958); **19**, 287 (1962).
[3] G. H. Rawitscher, Nucl. Phys. A **475**, 519 (1987).
[4] R. S. Mackintosh and N. Keeley, Phys. Rev. C **85**, 064603 (2012).
[5] N. Keeley and R. S. Mackintosh, Phys. Rev. C **97**, 014605 (2018).
[6] R. S. Mackintosh and N. Keeley, Phys. Rev. C **97**, 069901(E) (2018).
[7] R. S. Mackintosh and N. Keeley, Phys. Rev. C **98**, 024624 (2018).
[8] N. Keeley and R. S. Mackintosh, Phys. Rev. C **99**, 034614 (2019).
[9] N. Keeley and R. S. Mackintosh, Phys. Rev. C **77**, 054603 (2008).
[10] A. M. Kobos and R. S. Mackintosh, Acta Phys. Pol. B **8**, 887 (1977).
[11] I. J. Thompson, Comput. Phys. Rep. **7**, 167 (1988).
[12] D. Y. Pang, P. Roussel-Chomaz, H. Savajols, R. L. Varner, and R. Wolski, Phys. Rev. C **79**, 024615 (2009).
[13] J. S. Hanspal, R. J. Griffiths, and N. M. Clarke, Phys. Rev. C **31**, 1138 (1985).
[14] R. S. Mackintosh and N. Keeley, Phys. Rev. C **81**, 034612 (2010).
[15] N. Keeley and R. S. Mackintosh, Phys. Rev. C **90**, 044602 (2014).
[16] F. G. Perey and B. Buck, Nucl. Phys. **32**, 353 (1962).
[17] F. G. Perey, in *Direct Interactions and Nuclear Reaction Mechanisms*, edited by E. Clemental and C. Villi (Gordon and Breach, Science Publishers, New York, 1963), p. 125.
[18] R. S. Mackintosh and S. G. Cooper, J. Phys. G: Nucl. Part. Phys. **23**, 565 (1997).
[19] R. S. Mackintosh and N. Keeley, arXiv:1610.07378.
[20] I. Brida, S. C. Pieper, and R. B. Wiringa, Phys. Rev. C **84**, 024319 (2011).
[21] F. Flavigny, A. Gillibert, L. Nalpas, A. Obertelli, N. Keeley, C. Barbieri, D. Beaumel, S. Boissinot, G. Burgunder, A. Cipollone, A. Corsi, J. Gibelin, S. Giron, J. Guillot, F. Hammache, V. Lapoux, A. Matta, E. C. Pollacco, R. Raabe, M. Rejmund, N. de Séreville, A. Shrivastava, A. Signoracci, and Y. Utsuno, Phys. Rev. Lett. **110**, 122503 (2013).

[22] Y.-W. Lui, O. Karban, S. Roman, R. K. Bhowmik, J. M. Nelson, and E. C. Pollacco, Nucl. Phys. A **333**, 221 (1980).
[23] V. Avrigeanu, M. Avrigeanu, and C. Mănăilescu, Phys. Rev. C **90**, 044612 (2014).
[24] T. Kibédi and R. H. Spear, At. Data Nucl. Data Tables **80**, 35 (2002).
[25] E. Strano, D. Torresi, M. Mazzocco, N. Keeley, A. Boiano, C. Boiano, P. Di Meo, A. Guglielmetti, M. La Commara, P. Molini, C. Manea, C. Parascandolo, D. Pierroutsakou, C. Signorini, F. Soramel, D. Filipescu, A. Gheorghe, T. Glodariu, J. Grebosz, S. Jeong, Y. H. Kim, J. A. Lay, H. Miyatake, M. Nicoletto, A. Pakou, K. Rusek, O. Sgouros, V. Soukeras, L. Stroe, N. Toniolo, A. Vitturi, Y. Watanabe, and K. Zerva, Phys. Rev. C **94**, 024622 (2016).
[26] P. Doll, G. J. Wagner, K. T. Knopfle, and G. Mairle, Nucl. Phys. A **263**, 210 (1976).
[27] S. Raman, C. W. Nestor Jr., and P. Tikkanen, At. Data Nucl. Data Tables **78**, 1 (2001).
[28] R. S. Mackintosh and N. Keeley, Phys. Rev. C **90**, 044601 (2014).
[29] M. Matoba, K. Yamaguchi, K. Kurohmaru, O. Iwamoto, Susilo Widodo, A. Nohtomi, Y. Uozumi, T. Sakae, N. Koori, T. Maki, and M. Nakano, Phys. Rev. C **55**, 3152 (1997).
[30] A. Farooq, G. Rai, and S. Roman, Nucl. Phys. A **469**, 313 (1987).
[31] W. C. Parkinson, D. L. Hendrie, H. H. Duhm, J. Mahoney, J. Saundinos, and G. R. Satchler, Phys. Rev. **178**, 1976 (1969).
[32] F. Todd Baker and R. Tickle, Phys. Rev. C **5**, 544 (1972).
[33] Y. W. Lui, O. Karban, S. Roman, R. K. Bhowmik, J. M. Nelson, and E. C. Pollaco, Nucl. Phys. A **333**, 205 (1980).
[34] R. S. Mackintosh, Eur. Phys. J. A **53**, 66 (2017).